

Open-Source Hardware and Software for a Laboratory-Scale Track and Moving Vehicle Actuation System Used for Indirect Broken Rail Detection

Jeremy Yin^a, Guillermo Montero^a, Katherine A. Flanigan^{*a}, Mario Bergés^a, and James D. Brooks^b

^aDepartment of Civil and Environmental Engineering, Carnegie Mellon University, PA, USA

^bAdvanced Technologies, Wabtec Corporation, PA, USA

ABSTRACT

There is an urgent need to better understand vehicle-rail interaction dynamics to pave the way for more consistent and automated rail crack detection methodologies, as opposed to relying on periodic and manual detection via track circuits or dedicated track geometry cars. Designing an open-source hardware framework for a lab-scale rail testbed would open the doors to further data collection and analysis needed to understand the dynamic response of cracked rails. We present a framework and the corresponding open-source hardware and software (published to GitHub) for developing a laboratory-scale motorized railroad testbed, with a vehicle that is modularly tuned to the dynamics of an in-service rail car.

Keywords: Indirect monitoring, testbed development, rail damage simulation, scaled damage modeling

1. INTRODUCTION

Rail track defects and breaks are leading contributors to train derailments.¹ This potentially catastrophic mode of failure can have far-reaching consequences given that railroads, which amass nearly 140,000 route miles across the United States,² are a key transportation system on which the national economy is dependent. Railroads also have unique risk profiles as compared to other transportation systems because they support regional and national supply chains with little ability to reroute in the face of network closures. Moreover, since railroads are often operated by different for-profit corporations, rerouting must be coordinated across stakeholders. In 2020, the Federal Railroad Administration (FRA) estimated the value of the Class 1 freight rail industry at almost \$80 billion, with derailment-induced accidents leading to costly infrastructure and equipment losses, as well as economic costs for rail industry clients. While derailments lead to an average equipment and rail track damage cost of \$525,400 per incident on Class 1 railways, this does not include potential indirect costs such as damage to goods, hazardous waste cleanup, scheduling and supply chain disruption due to track outages, loss of future business, and loss of life, to name a few.³ Consequently, the ability to detect rail breaks in real time (i.e., as they occur) and automatically alert railroad officials is considered to be the “holy grail” of railroad track monitoring.

In recent years, laboratory-scale models have emerged to analyze the structural health of bridges, which has allowed researchers to more deeply understand the local and global dynamic characteristics of bridges. This advancement has ushered in the era of indirect structural monitoring, particularly for automobile- and truck-bridge interaction, where data collected from sensors installed onboard vehicles is used to draw conclusions about the health of the underlying structure.⁴ This line of work, which has now reached full scale, was originally built out from laboratory-scale testbeds that served as a solid foundation from which to better understand dynamic modeling and signal processing approaches.⁵ In principle, the same notion of indirect monitoring can, and has been, translated to railroads, where sensors are installed onboard train cars to detect track defects.⁶ Previous works have explored indirect monitoring strategies for full-sized vehicles through the use of GPS-accelerometers systems,⁷ laser vibrometer,⁸ and 3D LiDAR mapping.⁹ However, analyzing measured dynamic signals used to characterize and identify rail breaks is challenging due to the experimental reliance on full-scale trains, the

Further author information: (Send correspondence to K.A.F.)

K.A.F.: E-mail: kflaniga@andrew.cmu.edu, Telephone: 1 412 268 7274

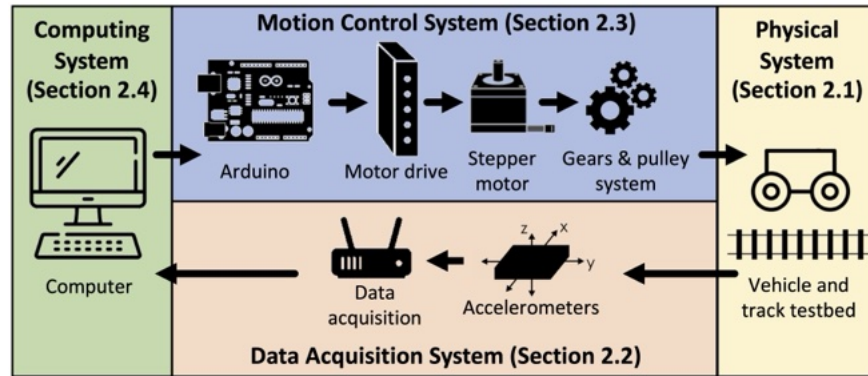


Figure 1. Overview of the high-level testbed system design, including functional relationships between key components.

noisiness of data resulting from vehicle-rail interactions, and the unreliability of accompanying real-world data. Despite these advancements, laboratory-scale railroad bridge testbeds that are tuned to replicate the in-service vehicle-rail interaction have not been well studied. There is an urgent need to better understand vehicle-rail interaction dynamics, starting with a realistic, laboratory-scaled model, to pave the way for more consistent and automated rail crack detection methodologies, as opposed to relying on periodic and manual detection via track circuits or dedicated track geometry cars.³ Designing an open-source hardware framework for a lab-scale rail testbed would open the doors to further data collection and analysis needed to understand the dynamic response of cracked rails.

To facilitate and expedite research progress in this area, we present a framework and the corresponding open-source hardware and software for developing a laboratory-scale motorized railroad testbed, with a vehicle and track that are tuned to the dynamics of an in-service railcar. Notably, this testbed is developed in collaboration with industry experts to ensure that the parameters and characteristics can capture real-world dynamics and behaviors. Specifically, the testbed comprises a 7.32m aluminum track, a vehicle operated by a belt system, a motion controller system, and a data acquisition system. Sampled data, software files, hardware design and assembly, and 3D CAD models are published to a GitHub repository.¹⁰ The testbed is based on a primitive experimental design used previously by the extended team to study vehicle-bridge interaction (VBI),¹¹ and has been radically redesigned to maximize its flexibility, accuracy, ease-of-use, and assembly, now including new modular components that allow researchers to study the structural responses of a plethora of to-scale track characteristics and defects. Additionally, the testbed is redesigned to model and study vehicle-rail interaction subjected to several types of broken rails. These adjustable components enable customization of the rail shape and break patterns. Working closely with rail industry experts, the testbed design features a vehicle with adjustable dimensions and weights to match a scaled version of a real-world rail car. We believe this publicly-available design specification for the testbed opens the doors for repeatable experiments that better define the dynamic responses of vehicle-rail interaction, and could significantly increase the pace of innovation in this space.

The remainder of the paper is organized as follows. Section 2 describes the experimental testbed and provides justifications for all modifications and tuned dynamic characteristics, as well as the mechanisms for simulating damage. This overview is decomposed into four primary design areas: the physical system, the data acquisition system, the motion control system, and the computing system. Section 3 presents sample data gathered from the testbed to illustrate its ability to simulate different rail conditions, along with the response they elicit on the rail car. Section 4 concludes with a summary of the testbed's capabilities and some recommendations for follow-on work.

2. TRAIN-TRACK SYSTEM

The developed testbed is subdivided into four primary systems, as shown in Figure 1. These comprise the physical system (i.e., the vehicle and track), the data acquisition system, the motion control system, and the computing

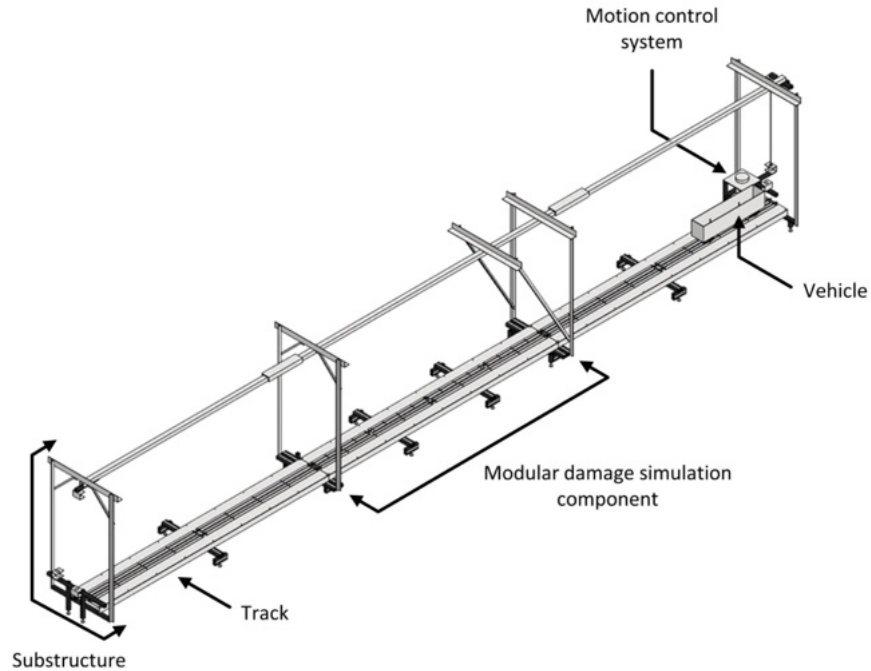


Figure 2. Schematic of the scaled testbed, including the underlying substructure and track, modular broken rail inserts, and vehicle. Here, the vehicle is located at the starting position.

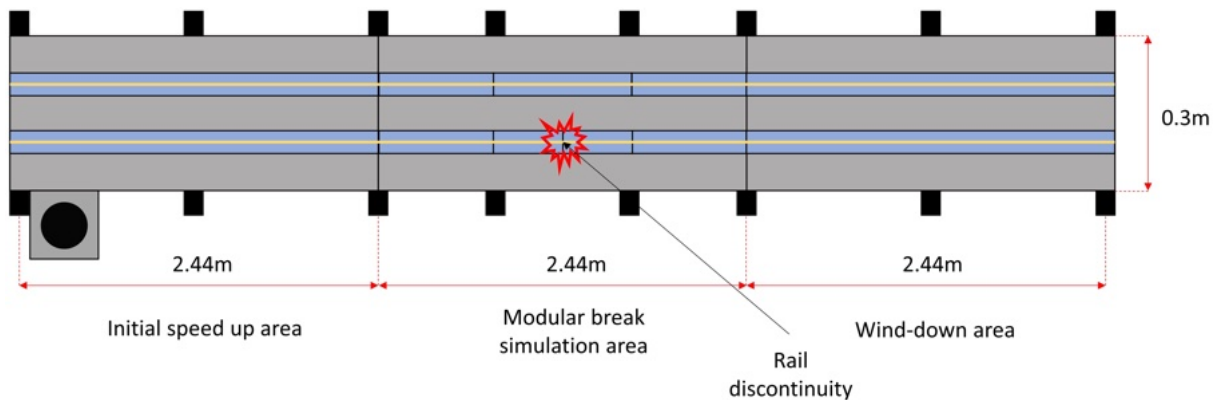


Figure 3. Schematic bird's-eye view of the three railtrack testbed sections.

system to coordinate the system and store the data. In the following sections, each of these components are discussed in detail, providing justifications for the design decisions made.

2.1 Physical system

The physical testbed (Figure 2) comprises three main components: the underlying substructure and track, the modular broken rail damage simulator, and the vehicle. The modularity of the design supports the investigation of the structural responses of a plethora of to-scale track characteristics and defects.

2.1.1 Substructure and track design

The function of the underlying substructure and track is to support the scaling and motorization of the vehicle, as well as to enhance the modularity and easy implementation of various broken rail patterns. The developed

Table 1. Comparison of the scaled and real-world velocities.

Down-scaled velocity (m/s)	Real-world velocity (km/hr) [miles/hr]
0.9	76.6 [47.6]
1.05	89.5 [55.6]
1.13	96.6 [60.0]
1.35	114.9 [71.4]

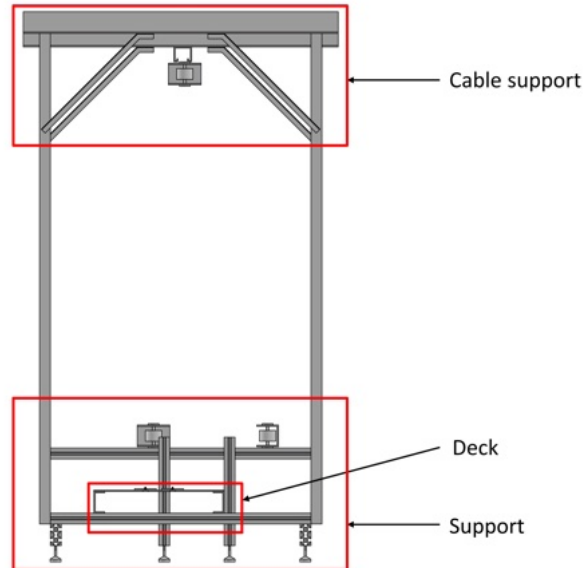


Figure 4. Schematic of the three vertical testbed layers.

testbed structure is made of aluminum, which is selected for its lightweight form, as well as its rust and corrosion-resistant characteristics as compared to steel, and its durability as compared to wood. The testbed, measuring 7.32m in length, is scaled with two main considerations: laboratory space and fabrication precision. The design length is limited by the available laboratory space designated for the project, which directly impacts the total length of the scaled testbed. The second limitation is the availability of in-house fabrication tools.

The testbed is divided into three 2.44m sections to allow for easy removal, relocation, and storage. As seen in Figure 3, these three sections also provide space for the initial vehicle speed up, break simulation, and vehicle wind down. The break simulation section, located in the central portion of the model, is where the damage is simulated. This section allows for the precise measurement of the dynamic response from the simulated damage, providing valuable insights into the behavior of rail systems under various damage conditions. The wind-down section allows the vehicle to slow down gradually, allowing for a smooth transition from the target peak velocity required for the simulation of the rail break back to the other end of the testbed. This section also helps to prevent any sudden changes in velocity that could affect the accuracy of the results obtained from the simulation, as well as to prevent damage to the belt propulsion system. To provide continuity in the rigidity of the rail where the simulated rail break is located, as well as to idealize the vehicle response, a single span is chosen rather than multiple spans. The testbed is primarily supported by three sets of two longitudinal 2.44m C-channels, which are placed under three $2.44 \times 0.3 \times 0.002$ m aluminum sheets to provide additional support to the decking. This design choice is made to ensure that the testbed remains stable during the simulation, without any excessive deformations or vibrations. Based on the literature documenting common rail break patterns,¹² damage is simulated through two disjoint rail sections that can be adjusted in three spatial coordinates. This

change allows for a more accurate simulation of rail breaks, providing valuable insights into their effects and helping to improve the design of rail systems.

Real-world train tracks have unique profiles that influence the vehicle's dynamic response. It is critical to use tracks that are precisely scaled and modeled to ensure proper simulation of the contact between the testbed structure and the testbed vehicle. This profile is very challenging to manufacture, so commercial scaled train components are used. Commercial standard replica train components come in many scales ranging from the Z-scale train with a ratio of 1:220 to the G-scale with a ratio of 1:24.¹³ To reduce the downscaling factor of the simulated rail breaks, the G scale, which is the largest commercially available scale, was chosen. The larger scale reduces human error and increases the accuracy of the simulated gaps by allowing for increased displacement tolerances compared to smaller scales. The initial speed-up section allows the vehicle to reach velocities ranging 0.9m/s to 1.35m/s, which correspond to a real-world range of 76.6km/hr to 114.9km/hr (Table 1).¹⁴

The testbed is also divided into three vertical layers: the support, decking, and cabling support. Figure 4 provides an overall schematic of these key testbed layers. Adjustable supports elevate the testbed from the ground, and the support height can be easily changed to ensure that the structure is level and uniformly supported. The decking, which supports the modular simulation components, comprises two aluminum C-channels, an aluminum sheet, an adjustable flat aluminum plates, and brass G-scale rails. An array of bolts secure the sheet on both sides to the underlying C-channels. Between each rail discontinuity on the deck layer (aside from the break simulation point), G-scale brass rail clamps hold the disconnected rails together to ensure perfect alignment of the rail profiles between sections. At the structure's highest point, the cabling layer contains a rigid channel spanning all three longitudinal sections, and holds the data transfer, power, and ground cables. A secondary belt system propels the cables at the same speed as the test vehicle to ensure that the cables do not snag or interact with the vehicle. This is made possible by a vertical shaft that connects one of the gears in the primary belt system to a gear up in the secondary system (illustrated at the far end of Figure 2).

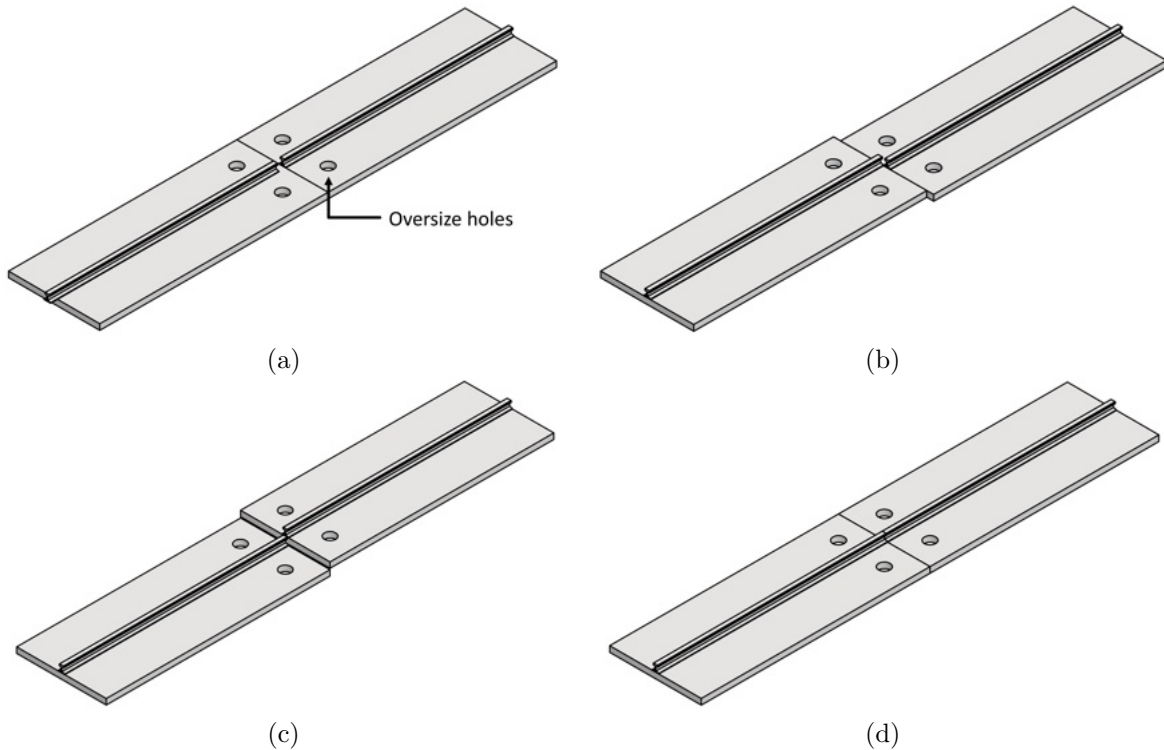


Figure 5. Rail crack simulations for (a) longitudinal, (b) lateral, (c) vertical, and (d) undamaged states.

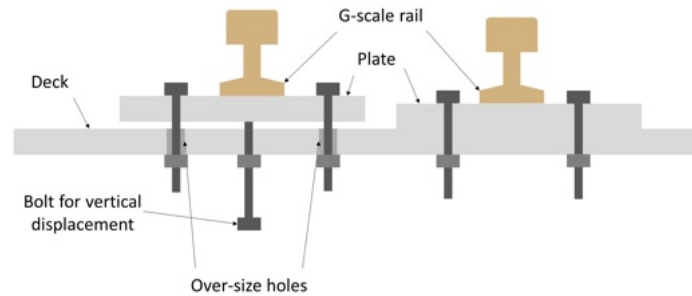


Figure 6. Schematic illustrating the modularity of the track design.

2.1.2 Damage simulation

The damage simulation is a critical component of the testbed, and involves three essential elements to simulate modular rail breaks in the longitudinal, lateral, and vertical directions (Figure 5). Recall from Figure 2 that the middle deck section is removable, enabling the insertion of different break pattern inserts. For each break pattern, the G-scale rail pieces are cut to size and fastened to the plate using two-part epoxy. When cut to precisely to 0.61m, the rail tracks sit flush against the rail piece on the opposing side of the gap to simulate unbroken, continuous rail (Figure 5(d)). Key elements supporting the modular design are illustrated in Figure 6.

First, in order to simulate longitudinal gaps, the undamaged rail-plate pieces can be easily replaced with inserts that have slightly shorter rails of varying gap sizes—ranging up to 2.55mm, which corresponds to real-world crack sizes of up to 60.3mm¹²—as seen in Figure 5(a). Second, oversized holes are drilled into the 2.4×0.3×0.002m aluminum sheet. Four pairs of oversized 6.35mm holes (Figure 5(a)) are cut in the center of each sheet to hold two 50.7×596.9×2mm aluminum plates in place. These holes are slightly larger than the 3.28mm diameter bolts used to fasten the plate to the deck but smaller than the 7.94mm hex nuts and provide some flexibility to simulate lateral breaks, as demonstrated in Figure 5(b). Lateral damage is displaced unilaterally away from the center of the testbed under the assumption that the slant found in real-world train wheels will push the rail outwards as it approaches a rail discontinuity. This assumption allows the testbed to simulate up to 0.4mm of lateral displacement, which corresponds to up to 9.6mm real-world transverse displacement.¹² Third, in order to simulate vertical displacement, a nut is glued under the oversize hole, allowing a bolt to be threaded through and push the track up. The more the bolt is threaded, the more it pushes up against the plate vertically, raising the plate and rail vertically to simulate vertical displacement as seen in Figure 5(c). The testbed can simulate up to 0.45mm of vertical damage, which corresponds to up to 10.6mm of real-world vertical displacement.¹²

2.1.3 Vehicle design

The testbed’s rail car, or “vehicle”, is modeled after a 15.4m boxcar¹⁵ and is scaled at a 1:23.65 ratio. This ratio results in a 2.5-inch rail gauge width and simplified fabrication. The 15.4m boxcar is selected as it is one of the shortest freight rail cars, enabling the vehicle to reach required speeds targeted for the break simulation given the laboratory’s space constraints. Longer vehicles will require a longer length of the initial speed-up section, necessitating a higher acceleration to reach the desired velocity before reaching the damage simulation section. Using the shortest industry standard rail car, the test vehicle can ease into the desired peak velocity while maintaining the short speed-up and wind-down sections.

Accurately modeling the rail car’s shafts and trucks is critical due to their influence on the vehicle’s dynamic response frequency and acceleration. The rail car’s wheel shaft and trucks are designed and scaled to match real-world dimensions,^{16–18} and are 3D printed with a Polylactic Acid (PLA) filament (Figure 7). The 3D-printed trucks comprise two separate components separated by four springs (two on each side), as shown in Figure 7(d). Each spring has a dynamically-scaled stiffness of 0.075kg/mm acting as a suspension system.¹⁶ As the trucks traverse the testbed’s track, the impact’s response is transferred through the suspension system into the box car where the accelerometers are installed. Due to the rough print lines resulting from the 3D printing process, the

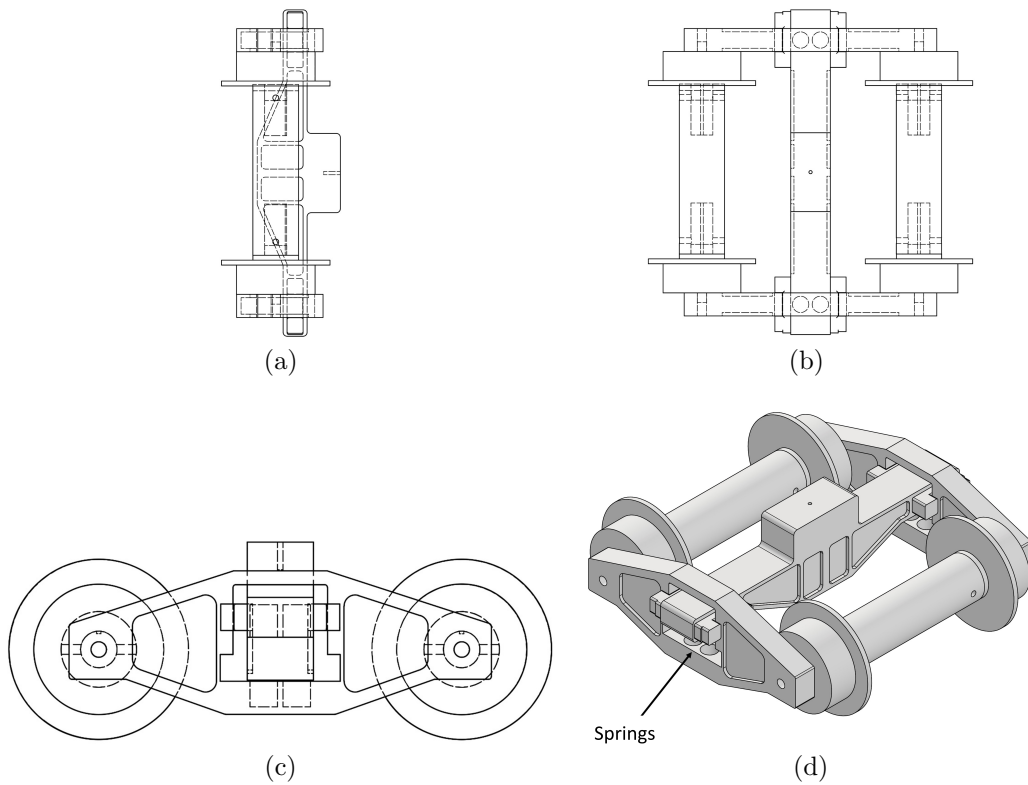


Figure 7. 3D printed model of the shaft and trucks including (a) front, (b) top, (c) side, and (d) isometric views.

trucks are sanded with 180-grit sandpaper to reduce friction between the parts. The shafts are printed to be thick and durable to provide rigidity and reduce any unwanted bending generated from the vehicle-track interaction. Real-world wheels have unique profiles that influence the vehicle's dynamic response. It is critical to use rail wheels that are precisely scaled and modeled to ensure proper simulation of the contact between the testbed structure and the testbed vehicle. This profile is very challenging to manufacture, so the model's wheels (shown in the Figure 8) are not 3D printed and, instead, are replaced by scaled commercial G-scale train wheels.^{17, 18}

The vehicle's box car is constructed from a steel plate, as shown in Figure 9. The sheet metal is cut to the desired dimensions and folded upward, creating the box car. The folded sides are then secured in place using L-brackets and fastened with bolts and nuts. To attach the steel box to the 3D-printed trucks, screws are threaded through the bottom of the metal box through a small wooden block and into the top of the truck. The small wooden block adds additional space so the bottom of the box will not hit the wheels. Additionally, four

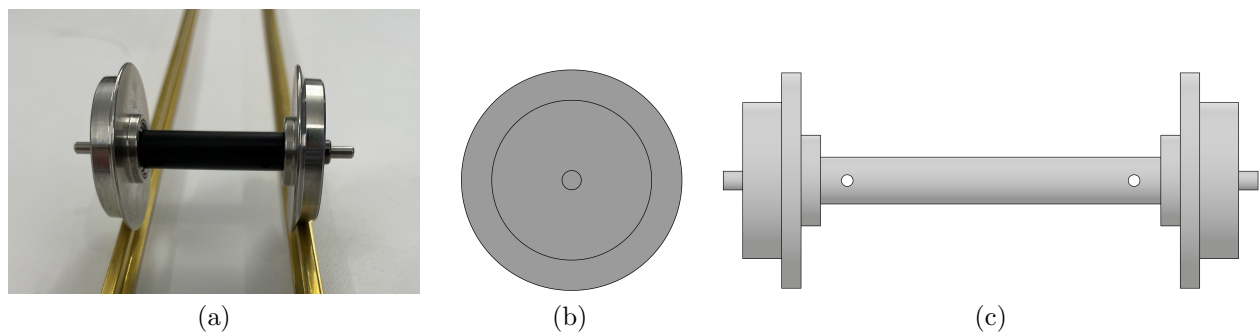


Figure 8. (a) G-scale train wheels, including schematic diagrams of the (b) side and (c) front views.

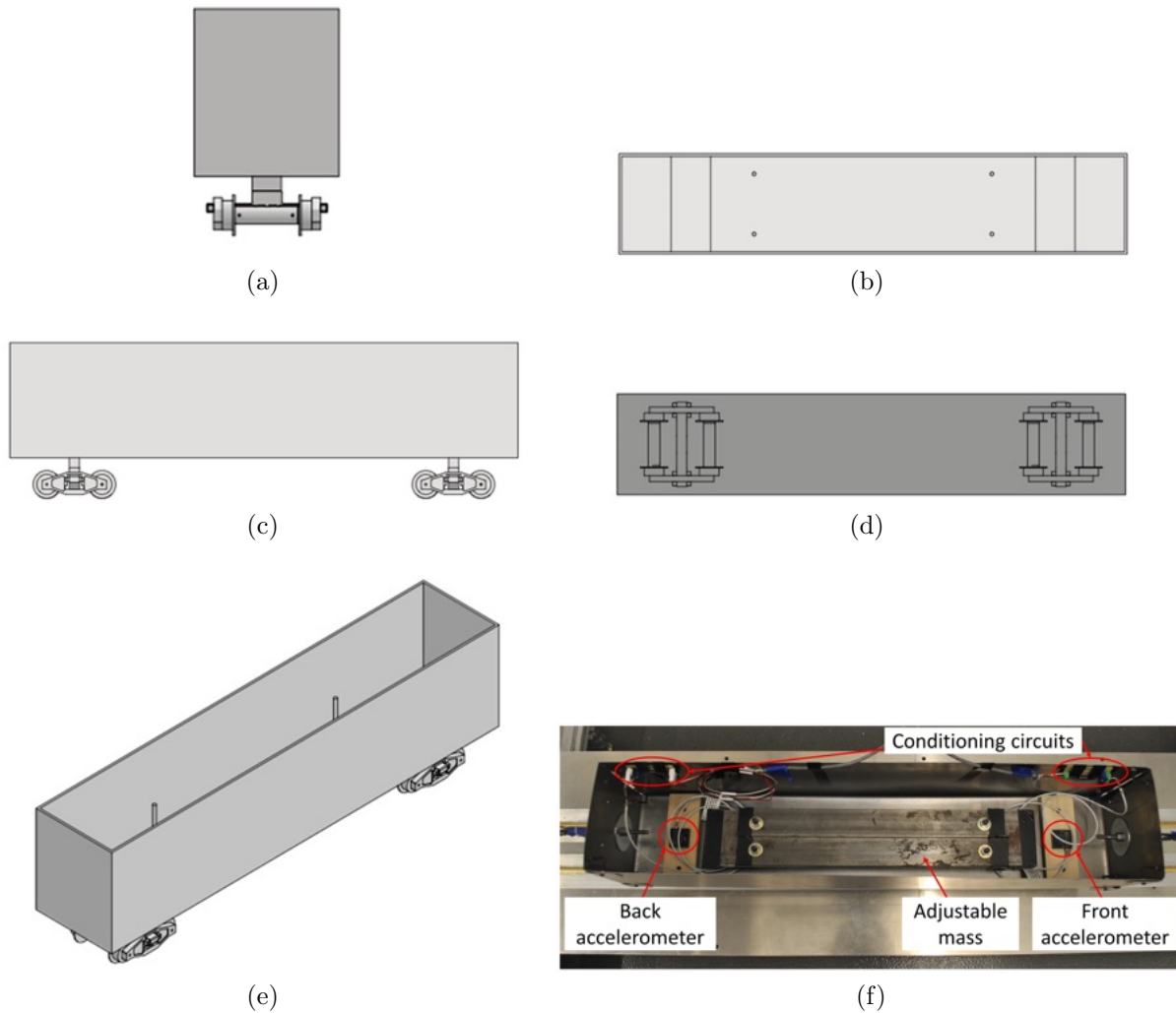


Figure 9. Model of the rail car, including (a) front, (b) top, (c) side, (d) bottom, and (e) isometric views, as well as (f) the fabricated model with key components highlighted.

thicker metal screws are fastened upwards from the bottom of the box car. These screws help hold pre-cut metal weights, weighing 1kg, 2.5kg, or 5kg (however other test weights can be considered), to the base of the rail car, which are typical weights of down-scaled 15.4m freight cars.¹⁵ Metal nuts and washers are tightened down to keep the added load from shifting around during the experiments.

As shown in Figure 9, two accelerometers, which will be discussed in Section 2.2, are secured to the wood blocks located within the box car above the trucks in order to isolate the sensors from the wheels. The sensors are also physically isolated to prevent potential ground loops from forming between the sensors due to the conductive metal box.

2.2 Data acquisition system

The testbed presented in this work uses two uniaxial $\pm 2g$ accelerometers manufactured by Silicon Design Inc.¹⁹ to measure acceleration in the vertical direction. As shown in Figure 9(f), Channel 0 corresponds to the sensor located in the back of the vehicle (i.e., the side closer to the motor) and Channel 1 refers to the sensor in the front. The response signal from the sensors undergoes conditioning via a custom-designed conditioning circuit with four primary features. The first feature is a trimming potentiometer that adjusts the output signal to a

range between 0V to 5V. To maximize the signal range and prevent thresholding, the baseline voltage is set to 2.5V. Secondly, switches onboard the circuit are used to adjust the signal's gain. In the field, smaller signals can be magnified prior to analog-to-digital conversion if the collected response is very small. Third, a low-pass Bessel filter eliminates high-frequency signal noise. Fourth, the board converts the differential signal from a double-ended to a single-ended output.

After passing through the conditioning circuit, the signal is transmitted through shielded cables that run along the top of the testbed to a USB-connected data acquisition system (National Instruments myDAQ²⁰). The myDAQ has a 16-bit 200kS/s analog-to-digital converter that is configured and managed via a custom LabVIEW²¹ graphical user interface on the computer.

2.3 Motion control system

The testbed's motion control system governs and carries out the vehicle's movement along the track. As previously discussed, the motion comprises three phases: the initial vehicle speed up, break simulation, and vehicle wind down. The motion control begins with LabVIEW software (described subsequently in Section 2.4), which commands a programmed microcontroller (Arduino Uno)²²—via a USA-A to USB-B cable—to run a custom script. The Arduino Uno, in turn, regulates a P70360 (AC) High Performance Micro-Stepping Drive²³ to turn the Pacific Scientific POWERPAC Hybrid Step Motor²⁴ with a Nema 34 frame at the speed specified by the LabVIEW input. Due to the precise nature of stepper motors, the stepping drive can control the motor to rotate at the correct, predetermined speeds.

The two connected belt systems regulate the motion of the test vehicle and the data transfer cables. The primary belt system is attached to the motor and rail car. By turning the motor clockwise, the rail car travels away from the stepper motor towards the end of the testbed. Conversely, turning the motor counterclockwise returns the vehicle to its starting position. A gear and shaft system transmits the rotation to a secondary belt system located on the top of the testbed, pulling the data acquisition wires resting on rolling hooks at the same speed as the vehicle. Doing so lessens the pulling exerted by the cables on the accelerometers in the vehicle.

2.4 Computing system

The computing system is responsible for controlling both the motion control and data acquisition systems. An Intel laptop runs the Windows operating system and a custom LabVIEW program. The LabVIEW program serves as the central coordinator for the testbed setup, as well as the graphical user interface for the testbed operator. The interface enables the user to configure the maximum velocity, control the sampling rate, specify

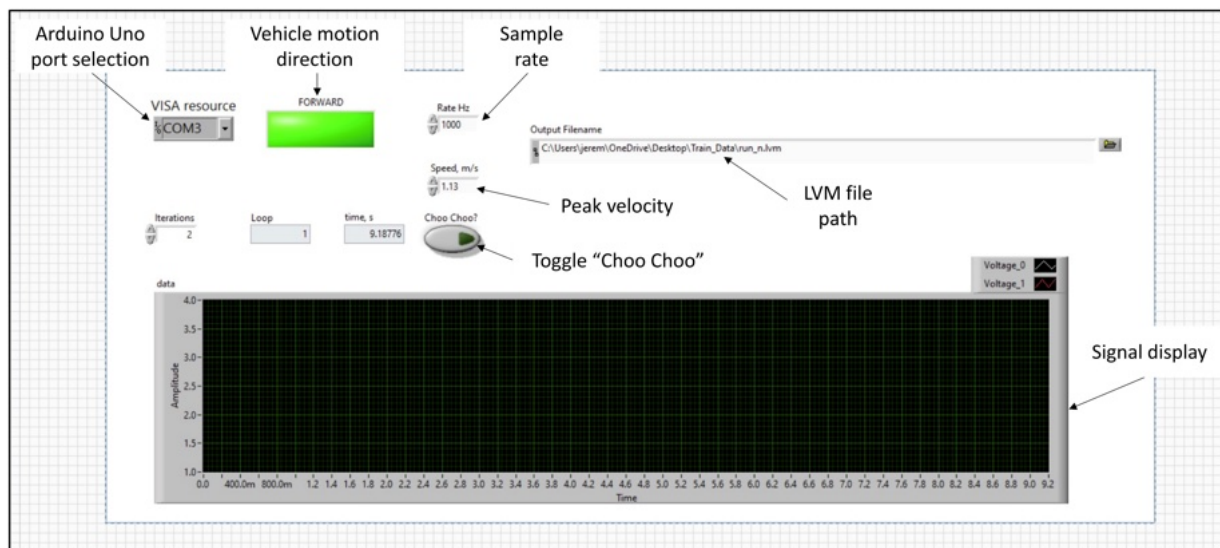


Figure 10. The LabVIEW user interface.

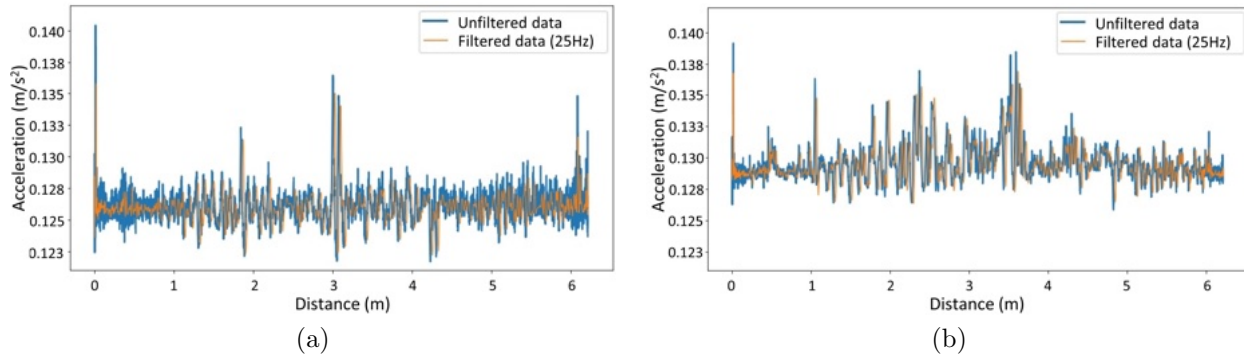


Figure 11. Low-pass filtered and unfiltered acceleration signals in the space domain for (a) Channel 0 and (b) Channel 1.

the file name for the captured data, and visualize the results for each run. The LabVIEW computing system ensures the stability of the rail vehicle's acceleration. Through its connection with the Arduino Uno, LabVIEW smoothens the rail vehicle's acceleration, preventing any abrupt changes that can cause the belt to skip and shift the starting and ending location of a run. LabVIEW operates the NI myDAQ data acquisition system and synchronously begins the data collection and the motion of the vehicle, allowing for consistency between experimental runs. Utilizing this interface, users have a comprehensive and user-friendly interface (Figure 10) that streamlines the data acquisition process while also providing a high level of control and customization.

At the end of each run, the LabVIEW program outputs data in the form of a LabVIEW Measurement (LVM) file. To ensure consistency, data is only collected when moving away from the stepper motor. An external Python script runs an auto-clicker that clicks on the run button at regular intervals. This reduces the need for human intervention between experimental setups. The output from the testbed intends to provide valuable information that can be used to further understand the effects of rail breaks and to improve the design of rail systems.

3. EMPIRICAL DEMONSTRATION OF THE TESTBED

To demonstrate the response of the vehicle, experimental data is collected under both damaged and undamaged scenarios. As previously discussed, the damaged cases can be simulated under longitudinal, lateral, and vertical displacement conditions. This section presents examples of preprocessed data, demonstrating how the results obtained can be used to ascertain whether any significant differences can be detected.

To preprocess the acceleration data, a linear transformation provided by the sensor's manufacturer is used to convert the voltage output into acceleration (m/s^2). Since the sensor collects data regardless of the vehicle's speed, the data is converted from the time domain into the space domain in order to be able to compare signals obtained with different speeds. The data is then passed through a 25 Hz low-pass Butterworth filter to remove the high-frequency noise content caused by the stepper motor's operational vibrations (Figure 11).

3.1 Space-domain data analysis

Sample runs are conducted using the damaged and undamaged conditions shown in Table 2. The acceleration signals are processed and shown in Figure 12 for both Channel 0 and 1. The analysis of the dynamic response of accelerometers has revealed that the front and back end of the vehicle experience different vibrational responses. This observation highlights the importance of the sensor location for effective damage detection in real-world applications. Furthermore, when comparing the time signals of the damaged and undamaged cases, there is no significant difference that can be easily discerned. This underscores the need for the development of algorithms capable of better interpreting the data using more sophisticated algorithms in order to successfully classify the different conditions of the rails.²⁵

Table 2. Experimental parameters for the damaged and undamaged runs.

	Undamaged runs	Damaged runs
Peak velocity (m/s)	0.9	0.9
Added mass (kg)	2.5	2.5
Longitudinal displacement (mm)	0	2.55
Lateral displacement (mm)	0	0.20
Vertical displacement (mm)	0	0.30

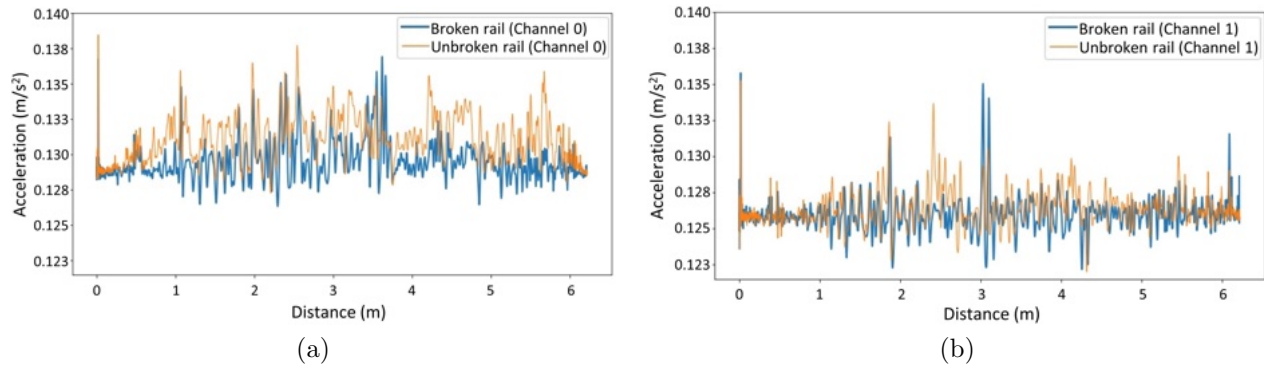


Figure 12. Comparison between the damaged and undamaged runs using the parameters outline in Table 2.

3.2 Frequency-domain data analysis

To gain further insight into the collected signals, the Fast Fourier transform (FFT) is performed on the data. This analysis is conducted with the aim of demonstrating any potential differences between the collected accelerations. Results for the broken rail runs are shown in Figure 13. Analyzing the FFT, it becomes apparent that the greatest differences are due to changes in the speed of the vehicle, rather than the simulated damage. The FFT analysis reveals more prominent peaks in the signals collected with higher vehicle speeds, indicating that the predominant frequency content of the signals gets more clear depending on the speed of the vehicle. Interestingly, the difference between Channel 0 and 1 is less evident in the frequency domain, suggesting consistency in the frequency content of the back and front vehicle's vibrations. This finding contrasts with the observation in the time domain signals, where the difference between the two channels was more noticeable. Hence, as previously mentioned, this data indicates that it is necessary to develop a damage detection methodology that can classify the damage condition of the rails, given the high variability of the signals given by factors that do not reflect damage, such as the speed of the vehicle.

4. CONCLUSIONS AND FUTURE WORK

Understanding rail defects and breaks is crucial, and a reliable method for studying these issues in a simulated environment can pave the way for real-time and low-cost railroad health monitoring. This paper proposes a laboratory-scaled testbed for rail damage simulation and detection to support indirect structural health monitoring. The testbed includes a detailed design of a 1:23.65 scaled structure and vehicle, discontinuity crack simulation in all three axes, and specific truck and shaft designs. The data acquisition, motion control, and computation systems are also described, along with sample acceleration signals in space domain and their corresponding FFT for four sets of damaged runs. General observations are performed on the processed signals and no substantial difference can be easily identified between damaged and undamaged runs. The greatest differences in the data are observed when the speed of the vehicle varies. For this reason, this work sets the stage for developing a reliable data processing scheme that can classify the different states of the lines. This proposed testbed can ultimately serve as a general framework for the down-scaling of model rail-vehicle structures to identify and prevent rail damage, thus enhancing the safety and reliability of rail transportation systems.

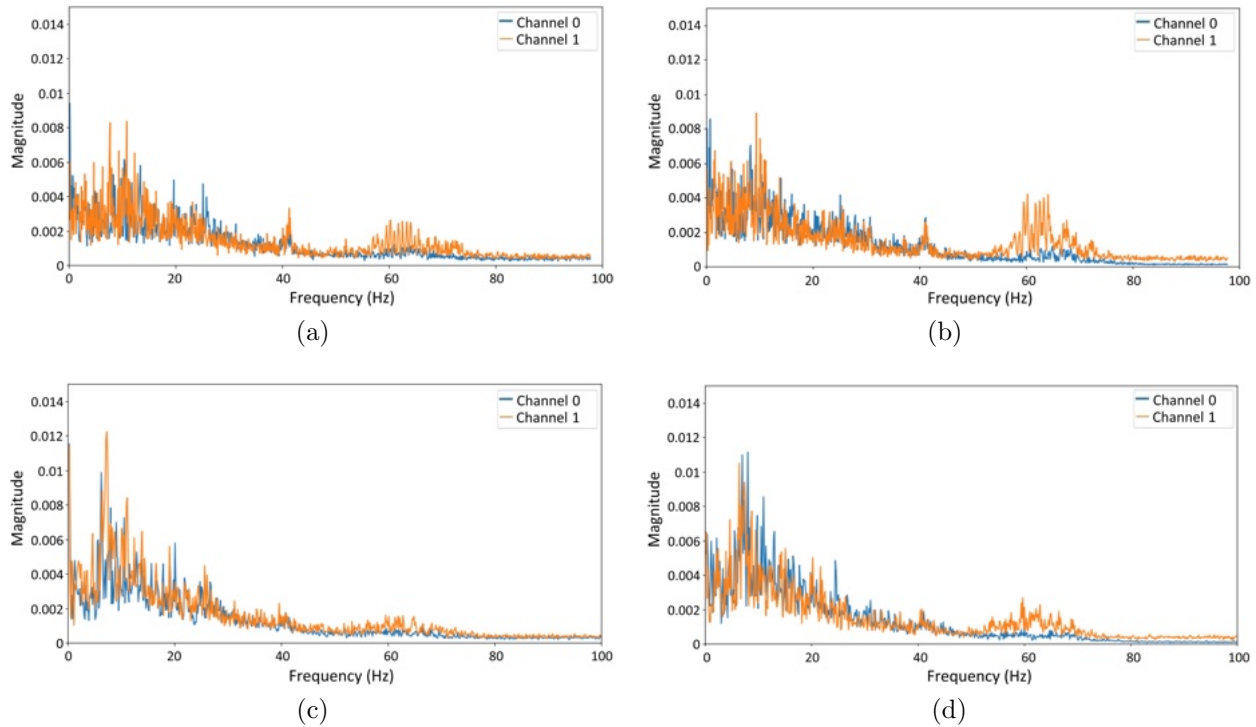


Figure 13. FFTs of the four damaged runs with (a) 0mm longitudinal displacement and 0.9m/s vehicle speed, (b) 2.55mm longitudinal displacement and 0.9m/s vehicle speed, (c) 0mm longitudinal displacement and 1.35m/s vehicle speed, and (d) 2.55mm longitudinal displacement and 1.35m/s vehicle speed.

ACKNOWLEDGMENTS

The authors would like to gratefully acknowledge Brian Belowich for his support in the development and fabrication of the testbed presented in this paper. This research is sponsored in part by the Pennsylvania Infrastructure Technology Alliance (PITA). Information developed under this Award was or is sponsored by the U.S. ARMY Contracting Command under Contract Number W911NF20D0002 and W911NF22F0014 delivery order No. 4.

REFERENCES

- [1] Liu, X., Saat, M. R., and Barkan, C. P. L., “Analysis of causes of major train derailment and their effect on accident rates,” *Transportation Research Record: Journal of the Transportation Research Board* **2289**(1), 154–163 (2012).
- [2] Federal Railroad Administration, “Freight rail overview.” <https://railroads.dot.gov/rail-network-development/freight-rail-overview>. [Online; accessed 02/18/2023].
- [3] Cannon, D. F., Edel, K., Grassie, S. L., and Sawley, K., “Rail defects: an overview,” *Fatigue & Fracture of Engineering Materials & Structures* **26**(10), 865–886 (2003).
- [4] Nie, Z., Lin, J., Li, J., Hao, H., and Ma, H., “Bridge condition monitoring under moving loads using two sensor measurements,” *Structural Health Monitoring* **19**(3), 917–937 (2020).
- [5] Malekjafarian, A., Corbally, R., and Gong, W., “A review of mobile sensing of bridges using moving vehicles: progress to date, challenges and future trends,” *Structures* **44**, 1466–1489 (2022).
- [6] Cerda, F., Garrett, J., Bielak, J., Bhagavatula, R., and Kovacevic, J., “Exploring indirect vehicle-bridge interaction for bridge SHM,” *Proceedings of the 5th International Conference on Bridge Maintenance, Safety, Management and Life-Cycle Optimization*, 696–702 (2010).
- [7] Malekjafarian, A., O’Brien, E., Quirke, P., and Bowe, C., “Railway track monitoring using train measurements: An experimental case study,” *Applied Sciences* **9**(22) (2019).

- [8] Malekjafarian, A., OBrien, E., and Cantero, D., “Railway track monitoring using drive-by measurements,” (10 2017).
- [9] Arastounia, M., “Automated recognition of railroad infrastructure in rural areas from LIDAR data,” *Remote Sensing* **7**(11), 14916–14938 (2015).
- [10] Yin, J., “Lab-Scaled-Open-Source Hardware.” <https://github.com/JeremyYin-99/Lab-Scaled-Open-Source-Hardware> (2023). [Online; accessed 02/23/2023].
- [11] Cerda, F., Garrett, J., Bielak, J., Rizzo, P., Barrera, J., Zhuang, Z., Chen, S., McCann, M. T., and Kovacevic, J., “Indirect structural health monitoring in bridges: scale experiments,” *Proceedings of the International Conference on Bridge Maintenance, Safety, and Management*, 706903 Bytes (2012).
- [12] Gao, Y., Wang, P., Kai, W., Xu, J., and Dong, Z., “Damage tolerance of fractured rails on continuous welded rail track for high-speed railways,” 59–73 (2020).
- [13] trains.com, “Model train scales explained.” <https://www.trains.com/mrr/beginners/model-train-scales-explained/>. [Online; accessed 02/18/2023].
- [14] Code of Federal Regulations, “Classes of track: operating speed limits.” <https://www.ecfr.gov/current/title-49/subtitle-B/chapter-II/part-213/subpart-A/section-213.9>. [Online; accessed 02/18/2023].
- [15] The Greenbrier Companies, “50’ plate F boxcar.” <https://www.gbrx.com/railcars/50-plate-f-boxcar/>. [Online; accessed 02/20/2023].
- [16] Harris, C. and Crede, C., [*Shock and vibration handbook*], Quality Press (1961).
- [17] Piko America LLC, “PIKO G-scale track.” <https://www.piko-america.com/collections/g-scale-g-track>. [Online; accessed 02/18/2023].
- [18] Piko America LLC, “PIKO G-Track for indoors and out.” https://cdn.shopify.com/s/files/1/1960/4221/files/99350_G-Track_Flyer.pdf?9757276037842777937. [Online; accessed 02/18/2023].
- [19] Silicon Designs Inc., “SDI 2012 & 2422 specialty +5V accelerometers.” <https://www.silicondesigns.com/2012-2422>. [Online; accessed 02/18/2023].
- [20] National Instruments Corp., “NI myDAQ specifications.” <https://www.silicondesigns.com/2012-2422>. [Online; accessed 02/18/2023].
- [21] National Instruments Corp., “LabVIEW.” <https://www.ni.com/en-us/support/downloads/software-products/download.labview.html#477380>. [Online; accessed 02/18/2023].
- [22] Arduino, “Arduino Uno Rev3.” <https://store-usa.arduino.cc/products/arduino-uno-rev3>. [Online; accessed 02/18/2023].
- [23] National Instruments Corp., “P70360 (AC) high performance micro-stepping drive.” <https://www.ni.com/pdf/manuals/P70360manual.pdf>. [Online; accessed 02/18/2023].
- [24] Pacific Scientific, “Pacific Scientific stepper motors.” <https://www.kollmorgen.com/en-us/products/catalogs/pacsci-step-sync-selection-guide-en/>. [Online; accessed 02/18/2023].
- [25] Montero, G., Yin, J., Flanigan, K., Bergés, M., and Brooks, J., “Anomaly identification algorithms for indirect structural health monitoring using a laboratory-scale railroad track system,” *SPIE Proceedings of Health Monitoring of Structural and Biological Systems XVII* (Mar. 2023).